Supplementary Information - Local chemotactic response of *Escherichia coli* in fluid and near surfaces

Adam Gargasson[1], Julien Bouvard[1], Carine Douarche[1], Peter Mergaert[2], Harold Auradou[1]

[1]Université Paris-Saclay, CNRS, FAST, 91405 Orsay, France

[2]Université Paris-Saclay, CNRS, I2BC, 91190 Gif-sur-Yvette, France

Correspondence: harold.auradou@universite-paris-saclay.fr

May 5, 2026

A Characterisation of the concentration gradient between the channels

To characterise the gradient between channel ① and channel ③, we repeated the experimental protocol, replacing the chemoattractant with fluorescein. Additionally, a lower magnification objective was used to enable simultaneous visualisation of all three channels. Fig. 1a) shows an image acquired after several minutes of injecting dye into channel ① and dye-free water into channel ③.

To quantify the dye concentration profile across the two channels, the image greyscale intensity was averaged along the x-direction. Figure 1b) illustrates the profiles obtained by analysing an image sequence that begins when the flow in channel ② is stopped, with a flow rate of 1 µL/min maintained in channels ① and ③. We observe that the light intensity in channel ② increases over time. Additionally, a gradient forms and, after a few minutes, stabilises into a constant gradient characterised by a linear evolution in light intensity across channel ②. Meanwhile, the light intensity in channel ① remains unchanged, whereas that in channel ③ shows a slight increase. To characterise the time required for the intensity profile to establish, we calculated the average light intensity in channel ②. This value is plotted in Fig. 1c) as a function of time.

We will now compare our observations with the analytical solution for the concentration profile between two boundaries separated by a distance L, where the concentrations are fixed at c_1 (at $y = 0$) and c_3 (at $y = L$).

The variation in concentration between channel ① and channel ③ follows Fick's law:

$$\partial_t c = -D\partial_y^2 c \tag{1}$$

The solution of this equation for a finite domain [0,L] with Dirichlet boundary conditions:

$$c(0,t) = c_1; \tag{2}$$

$$c(L,t) = c_3 \tag{3}$$

and an initial condition:

$$c(x,0) = 0 \tag{4}$$

can be derived using a Fourier series expansion [1]. At short times: The first term of the Fourier series dominates the dynamics, and the solution can be approximated by:

$$\frac{c(y,t) - c_1}{c_3 - c_1} \approx \frac{y}{L} + \frac{2}{\pi}\sin\left(\frac{\pi y}{L}\right) \cdot e^{-D_{\text{med}}^{\text{fluo}}\left(\frac{\pi}{L}\right)^2 t}, \tag{5}$$

where $D_{\text{med}}^{\text{fluo}}$ is the diffusion coefficient of fluorescein in the medium. The average concentration between the two channels: $\bar{c}(t) = (1/L)\int_0^L c(y,t)dy$ gives:

$$\frac{\bar{c}(t) - c_1}{c_3 - c_1} \approx \frac{1}{2} + \frac{4}{\pi^2} e^{-D_{\text{med}}^{\text{fluo}}\left(\frac{\pi}{L}\right)^2 t} \tag{6}$$

The characteristic time required to reach a steady-state regime, where the average concentration $\bar{c}$ remains constant, is $L^2/(\pi^2 D)$. This time can be determined experimentally by analysing the curve that illustrates the changes in average light intensity in the central channel, as shown in Fig. 1c). The exponential fit (solid line in Fig. 1c) indicates a time of 24 min. For a length $L = 1000$ µm, this results in a molecular diffusion coefficient $D_{\text{agar}}^{\text{fluo}} = 70\,\mu\text{m}^2/\text{s}$, which is lower than the value of $D_{\text{water}}^{\text{fluo}} = 430\,\mu\text{m}^2/\text{s}$ reported for diffusion in water [2, 3].

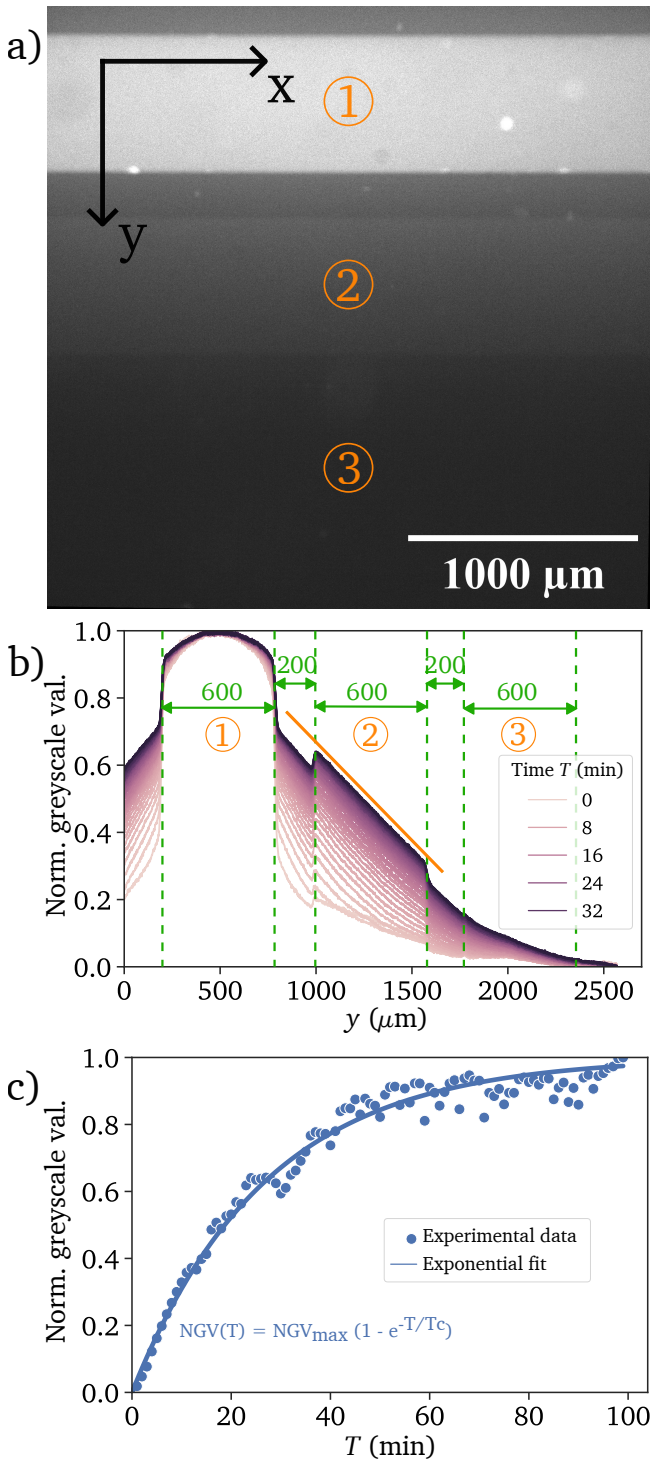

Figure 1: a) Image showing the three channels after $T = 100\,\text{min}$. The image was captured under fluorescence at 5× magnification. b) Spatial profile of the normalised greyscale value averaged over x measured at different times. c) Time evolution of the normalised greyscale value in channel ②. Fluorescein solution is injected into channel ① at $T = 0$ at a rate of 1 µL/min. Pure water is injected into channel ③ at $T = 0$ at the same rate of 1 µL/min. The flow is stopped in channel ② at $T = 0$. The time evolution is fitted with an exponential law: $\text{NGV}(T) = \text{NGV}_{\max}(1 - e^{-T/T_c})$, with $T_c = 24\,\text{min}$ the characteristic diffusion time.

Several factors explain the reduction of the diffusion coefficient of the fluorescein observed in agar. These include interactions between the hydrogel network and the solute, as well as obstacles to solute transport created by the hydrogel matrix [4–6].

Note that the concentration gradient ∇c used throughout the article was calculated based on the concentrations c_1 and c_3 in the lateral channels where a constant flow is maintained, i.e. $\nabla c = (c_3 - c_1)/L$. Thus, ∇c is based on the assumption that a perfectly linear concentration profile is established between channels ① and ③. The concentration profile of fluorescein in Fig. 1b) suggests that this formula overestimates the gradient by 40 %. However, this concentration profile, whose main objective is to confirm the linearity of the steady gradient, has itself a few caveats, e.g. the integration of light intensity through the z-axis, which is why we did not correct the theoretical value of the gradient when calculating the chemotactic susceptibility χ.

The chemoattractants used in our experiments are not visible under fluorescence. We will assume that molecular size is the most critical factor determining the diffusion coefficient. If the molecules are of comparable size, we will further assume that they diffuse through the hydrogel with the same dynamics. To estimate the size of the molecules in the casamino acids mixture, we considered it to be composed of an equimolar distribution of 20 amino acid molecules. Based on this assumption, we calculated an average Stokes radius of approximately 4.2 Å. MeAsp is an amino acid. Its radius can be estimated from aspartate's radius as ≈ 4 Å [7]. These values are comparable to the size of the fluorescein molecule (≈ 5 Å) [2, 3].

It is important to note that chemoattractant consumption by bacteria is neglected in Eq. (1). This is obvious for MeAsp, which is not metabolised by *E. coli*. However, casamino acids are. The approximation will thus be only valid if the consumption rate of the constituents of the casamino acids by the bacteria does not exceed the rate at which they are replenished by diffusion from the lateral channels.

The casamino acids are consumed at a rate below $0.05\,\mu\text{M}/(\text{OD}\,\text{s})$ [8]. In our experiments, OD ≈ 0.08, and $\bar{c} < 3 \times 10^5\,\mu\text{M}$ yielding a characteristic consumption time of 1.25×10^6 min. This duration is significantly longer than the ∼ 24 min required to establish a gradient. Therefore, the metabolisation of the casamino acids can be neglected as well.

Another critical timescale is the time required for chemoattractants to diffuse from the agar into channel ② and for a gradient to establish across the width of the channel. The transition from a state in which the

channel contains no chemoattractant to one in which a gradient is fully established occurs via molecular diffusion. The characteristic time for this process is $\tau_D = h^2/(2D^{\text{chemo}}_{\text{water}}) \approx 15\,\text{s}$, with $D^{\text{chemo}}_{\text{water}} \approx 500\,\mu\text{m}^2/\text{s}$ the diffusivity of the chemoattractants in water based on their Stokes radii. This timescale is 100 times shorter than the time required to establish the gradient within the agar layer between channels ① and ③ (see Fig.1). This difference arises from the aspect ratio: the channel height $h = 120\,\mu\text{m}$ is much smaller than its $600\,\mu\text{m}$-width.

B Effect of the chemoattractant concentration and gradient on the swimming velocity and motility

To investigate the impact of chemoattractants on bacterial motility, we analysed each video to quantify the bacterial swimming velocity v_s and the trajectory correlation time τ. The same analysis was performed on experiments without chemoattractants to determine their influence on bacterial motility.

Figure 2 displays the averaged values of v_s and τ from seven time-lapse images recorded at $z = h/2$ during each experiment. The vertical bars represent the quadratic deviation over the seven values measured. In the figures, the values obtained for the experiments conducted without a chemoattractant are shown with a dotted line and a grey background. Each symbol denotes a unique batch of bacteria, making measurement variations likely due to differences between batches.

Solute	v_s (μm/s)	τ (s)	μ (μm^2/s)
ø	12 ± 3	2.0 ± 1.0	290 ± 200
Cas. acids	14 ± 3	2.2 ± 1.0	430 ± 200
MeAsp	11 ± 1	3.3 ± 0.8	400 ± 100

Table 1: Swimming velocity v_s, correlation time τ, and diffusion coefficient μ in the absence of chemoattractant (ø), with casamino acids (Cas. acids) and with α-methyl-DL-aspartic (MeAsp). The values are the averages over all time-lapse images taken at half-height, $z = h/2$, in the channel.

Table 1 gives the values of the swimming velocity and correlation time averaged over all the experiments performed with or without chemoattractants. The diffusion coefficients μ derived from the equation $\mu = v_s^2\tau$ are consistent with the range reported in the literature (see, for example, Tab. 2 in [9] or [10]). Our results indicate no significant variation in either the correlation time or the swimming velocity with $\bar{c}$. However, a slight dependence on the chemical nature of the attractant is observed: the correlation time is approximately 1 s longer in MeAsp compared to casamino acids or in the absence of a chemoat-

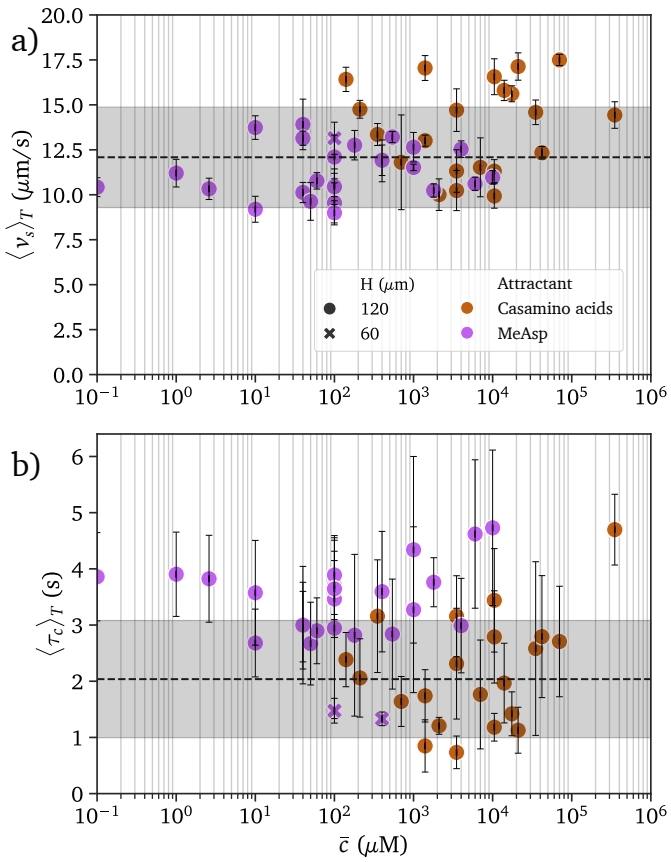

Figure 2: Bacterial motility characteristics a) Bacterial swimming velocity $\langle \bar{v}_s \rangle_T$ and b) average correlation time $\langle \tau \rangle_T$ estimated from the velocity correlation function, as a function of chemoattractants concentration. Purple and orange markers correspond respectively to MeAsp and casamino acids. The average is done over all the image sequences recorded during one experiment. Horizontal dashed lines and grey strips: average and range of variation for three experiments without chemoattractant ($c_1 = c_3 = 0\,\text{mM}$). Vertical bars indicate the second moment of the time distributions.

tractant. Concurrently, the swimming velocity is found to be 2 µm/s higher in casamino acids than in MeAsp or with out chemoattractant conditions. Ultimately, due to the opposing effects, the diffusion coefficient in MeAsp is comparable to that measured in the absence of chemoattractants (see Table 1).

C Verification of the shallow gradient assumption

A series of experiments was conducted to verify the shallow gradient limit in our studies and to validate the use of Eq.(2). To achieve this, the values of c_1 and c_3 were adjusted so that the average concentration $\bar{c}$ remained constant, while the gradient varied. Fig. 3 shows the normalised averaged chemotactic velocity $\tilde{v}_c$ as a function of the imposed gradient. The data points align on a straight line with a slope of $\chi = 0.75\,\mu\text{m}/\mu\text{M}$. Based on this result, we see that the chemotactic susceptibility can be obtained from the measurement of v_c knowing the imposed gradient ∇c as: $\chi(\bar{c}) = v_c/\nabla c$.

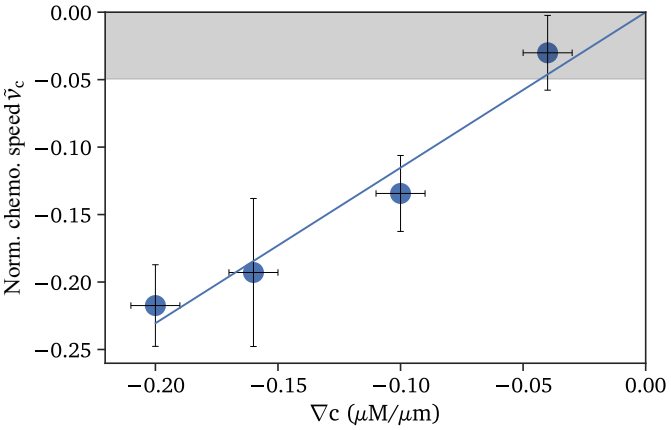

Figure 3: Normalised chemotactic velocity $\langle \tilde{v}_c(T) \rangle_T$, averaged over all times T, as function of ∇c measured for an average MeAsp concentration of $\bar{c} = 100\,\mu\text{M}$. The solid line is a linear fit of the data by $\tilde{v}_c = \chi \nabla c$ with $\chi = (0.72 \pm 0.05)\,\mu\text{m}/\mu\text{M}$. The vertical bars represent the second moment of the distribution of $\tilde{v}_c(T)$.

D Changes in bacterial profiles observed over time-lapse images

Eq.(1) represents the balance between the different fluxes present, specifically the chemotactic and diffusive fluxes, and accounts for flux variations in both space and time. Our method focuses on determining fluxes from analysed tracks generated from 20 seconds of time-lapse images. We assume that the flux remains relatively constant during this 20-second interval. This assumption is equivalent to the time-separation condition used in statistical physics to describe how a system evolves toward equilibrium. The time separation condition implies that correlations between the system's states at two widely separated times decay. This allows us to describe how microscopic interactions lead to macroscopic properties over time.

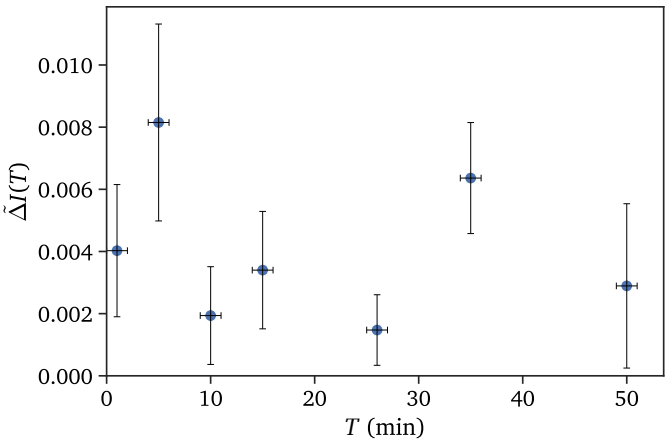

Figure 4: Root-mean-square (RMS) of the difference between the x, t-averaged light profiles along y at $z = h/2$ measured for the 7 image sequences in a single experiment, as a function of time T.
Here, $\tilde{\Delta}I(T) = \left\langle 2\dfrac{I(T, t > 15\,\text{s}, y) - I(T, t < 5\,\text{s}, y)}{I(T, t < 15\,\text{s}, y) + I(T, t > 5\,\text{s}, y)} \right\rangle_y$.

To quantify this point, we analysed the evolution of the bacterial profile over 20 s using the 200 frames that compose each time-lapse. First, the intensity of each frame was averaged along the x-direction. The first 50 profiles were then averaged, and the same operation was performed on the last 50 profiles obtained from the final 50 frames of the time-lapse. The evolution between the beginning and end of the sequence was quantified using the root-mean-square (RMS) of the difference between the two normalised profiles. This value was measured for the 7 image sequences in a single experiment. Fig. 4 shows the measured value as a function of T. This quantity remains consistently below 1 %, demonstrating that the bacterial profile changes minimally between the start and end of a film. This observation holds throughout the experiment, even as the bacterial profile transitions from a constant distribution to an exponential one. This measurement validates the time-separation condition and confirms that the system's macroscopic evolution can indeed be described from microscopic results.

References

[1] J. Crank, The mathematics of diffusion, Oxford university press, 1979.

[2] M. B. Mustafa, D. L. Tipton, M. D. Barkley, P. S. Russo and F. D. Blum, Macromolecules, 1993, **26**, 370–378.

[3] N. R. Richbourg and N. A. Peppas, Macromolecules, 2021, **54**, 10477–10486.

[4] B. Amsden, Macromolecules, 1998, **31**, 8382–8395.

[5] L. Masaro and X. Zhu, Progress in Polymer Science, 1999, **24**, 731–775.

[6] E. Axpe, D. Chan, G. S. Offeddu, Y. Chang, D. Merida, H. L. Hernandez and E. A. Appel, Macromolecules, 2019, **52**, 6889–6897.

[7] S. Liu, X. Xiang, X. Gao and H. Liu, Scientific Reports, 2020, **10**, 4371.

[8] A. Ganesh, Theses, Université Paris-Saclay, 2023.

[9] P. Lewus and R. M. Ford, Biotechnology and Bioengineering, 2001, **75**, 292–304.

[10] T. Ahmed, T. S. Shimizu and R. Stocker, Nano Letters, 2010, **10**, 3379–3385.